Changes in Observed Daily Precipitation over Global Land Areas since 1950

STEEFAN CONTRACTOR,[a] MARKUS G. DONAT,[b] AND LISA V. ALEXANDER[c]

[a] *School of Mathematics and Statistics, University of New South Wales Sydney, Sydney, New South Wales, Australia;* [b] *Barcelona Supercomputing Centre, Barcelona, Spain;* [c] *Climate Change Research Centre and ARC Centre of Excellence for Climate Extremes, University of New South Wales Sydney, Sydney, New South Wales, Australia*

(Manuscript received 19 December 2019, in final form 27 August 2020)

ABSTRACT: Estimates of observed long-term changes in daily precipitation globally have been limited due to availability of high-quality observations. In this study, a new gridded dataset of daily precipitation, called Rainfall Estimates on a Gridded Network (REGEN) V1–2019, was used to perform an assessment of the climatic changes in precipitation at each global land location (except Antarctica). This study investigates changes in the number of wet days (≥1 mm) and the entire distribution of daily wet- and all-day records, in addition to trends in annual and seasonal totals from daily records, between 1950 and 2016. The main finding of this study is that precipitation has intensified across a majority of land areas globally throughout the wet-day distribution. This means that when it rains, light, moderate, or heavy wet-day precipitation has become more intense across most of the globe. Widespread increases in the frequency of wet days are observed across Asia and the United States, and widespread increases in the precipitation intensity are observed across Europe and Australia. Based on a comparison of spatial pattern of changes in frequency, intensity, and the distribution of daily totals, we propose that changes in light and moderate precipitation are characterized by changes in precipitation frequency, whereas changes in extreme precipitation are primarily characterized by intensity changes. Based on the uncertainty estimates from REGEN, this study highlights all results in the context of grids with high-quality observations.

KEYWORDS: Atmosphere; Land surface; Extreme events; Precipitation; Climate change; Climate variability

1. Introduction

Changes in precipitation may have far-reaching impacts on global food production, industry, infrastructure, human health and well-being, geopolitical stability and human security, and natural ecosystems. For example, a decrease in precipitation frequency can lead to droughts and an increase in intensity can lead to floods. Precipitation is expected to intensify globally in the context of a warming climate, since the Clausius–Clapeyron (CC) relationship states that the moisture-holding capacity of air increases with temperature (Allen and Ingram 2002; Trenberth 1999, 2011). However, the exact nature of this change in precipitation is still not completely understood. For example, despite an increase in global mean precipitation, regional variation in the direction and strength of changes may exist (O'Gorman 2015; Trenberth 2011; Held and Soden 2006). Furthermore, different parts of the precipitation distribution may exhibit different rates of temporal changes (Alexander et al. 2007). Based on an assesment of existing studies, the IPCC's Fifth Assessment Report (AR5) (Hartmann et al. 2013) assigned ''low confidence'' to historical precipitation changes in many regions citing issues related to data availability, lack of studies, and conflicting results—for example, in India (Bhutiyani et al. 2010; Kishore et al. 2016; Mondal et al. 2015; Jain et al. 2013; Guhathakurta and Rajeevan 2008), South Africa (MacKellar et al. 2014; Kruger 2006; Kruger and Nxumalo 2017; Groisman et al. 2005), northwestern, sub-Saharan, and central-western Africa (Hulme et al. 2001; New et al. 2006; Aguilar et al. 2009; Chaney et al. 2014), the Horn of Africa (Tierney et al. 2015; Omondi et al. 2014; Liebmann et al. 2014), Iran (Zhang et al. 2005; Rahimzadeh et al. 2009), and Southeast Asia (Caesar et al. 2011; Limsakul and Singhruck 2016; Manton et al. 2001; Mayowa et al. 2015). Arguably, the paucity of long-term observations of daily precipitation is the primary reason behind the IPCC's assessment, because the lack of data can explain the lack of studies and conflicting results in many regions. For example, the conflicting changes depicted in many studies are due to a dissimilar network of stations used (e.g., in South Africa; northwestern, sub-Saharan, and central-western Africa; Iran; and Southeast Asia).

Studies based on monthly datasets of precipitation have been unable to capture changes in the extreme (wet) tails of the distribution since they flatten the daily extremes. Monthly (gauge-based) datasets usually have the advantage of benefiting from a more complete station network, compared to daily precipitation datasets, extending back to the start of the twentieth century. The longer time period of monthly data makes them ideal for investigating climate-related variability in precipitation. For example, IPCC AR5 compared trends in monthly precipitation anomalies averaged globally and over latitudinal bands between five monthly datasets (Peterson and Vose 1997; Adler et al. 2003; Mitchell and Jones 2005; Becker et al. 2013; Smith et al. 2012). The assessment found no significant trends in all five datasets after 1950 but significant positive trends were found since 1900 with large variance in the magnitudes of trends between datasets. Another study by Trenberth (2011) used monthly satellite data (Huffman et al. 2001) to show that in general precipitation has increased in the subtropics and the tropics outside the monsoon trough and decreased in the high latitudes (notably over North America, Europe, Asia, and Argentina). While they provide relatively

Corresponding author: Steefan Contractor, s.contractor@unsw.edu.au

DOI: 10.1175/JCLI-D-19-0965.1

long and spatially complete data, these monthly observational datasets, however, do not resolve the daily variability in data and flatten the daily or higher frequency extremes. For this reason, daily data are necessary to get a more accurate estimate of precipitation changes. Few studies have investigated global changes in precipitation using daily observations because of the limited availability of long-term datasets of daily precipitation that would allow the investigation of climate-scale changes. Existing global datasets of daily precipitation either are satellite-based and hence are limited to the satellite era (1979 onward) or, with reference to gauge-based datasets, suffer from data sharing issues between countries, resulting in the short temporal records extending back to around 1980 at best.

To overcome some of these data limitations, the Expert Team on Climate Change Detection and Indices (ETCCDI) proposed a set of climate indices (Zhang et al. 2011a; Peterson and Manton 2008), as data providers from some countries were more willing to share derived measures rather than daily data. Data collections of such station-based indices were then used as the basis for quasi-global gridded datasets allowing the study of some specific aspects of observed precipitation (and temperature) extremes. Examples of such global gridded datasets of indices created in this way are HadEX (Alexander et al. 2006), HadEX2 (Donat et al. 2013b), and GHCNDEX (Donat et al. 2013a). Based on all these datasets, precipitation indices show more areas with a significant shift toward wetter conditions compared to areas with a significant shift toward drying conditions. The most notable areas with trends toward wetter conditions were eastern North America, eastern Europe, Asia, and South America. Most recently Donat et al. (2016) used HadEX2 and climate model simulations from the archive of phase 5 of the Coupled Model Intercomparison Project (CMIP5; Taylor et al. 2012) to show statistically significant increases in extreme precipitation in both wet and dry regions of the world, while annual total precipitation also increased in the dry regions but not in the wet regions. Studies based on these indices, however, only investigate changes in very specific aspects of the precipitation distribution such as the means and the extreme tail. To gain a more comprehensive understanding of how precipitation is changing, changes in the entire distribution must be analyzed, for example, as demonstrated for Australia by Contractor et al. (2018).

Some studies, such as those of Groisman et al. (2005) and Westra et al. (2013), have not used gridded precipitation data, which can result in spatial biases due to the inhomogeneous distribution of stations. Groisman et al. (2005) used a subset of around 32 000 stations from the Global Daily Climatology Network and showed that the frequency of the heavy and very heavy precipitation events (top 10% and top 5% of events) has gone up in North America, eastern Europe, Scandinavia, Russia, China, India, Southeast Asia including Australia, southern and western Africa, and Brazil. Westra et al. (2013) used the same dataset of global land-based stations used to create HadEX2 to show that two-thirds of stations showed statistically significant increasing trends in annual extremes and that this result was inconsistent with the null hypothesis that there was no trend in precipitation extremes.

Besides the global studies a number of regional studies have also been conducted; however, large gaps in high confidence changes remain in many global regions. Based on our assessment, high confidence changes in the literature were found only in regions with high-quality long-term observations such as Europe, Australia, China, North America, and parts of South America (Fig. 1). The regions of high confidence changes in this assessment were defined as those regions with at least two studies showing significant increases or decreases and no other studies showing contradicting significant changes. Our assessment classified changes in precipitation over the twentieth century into frequency, intensity, and total changes in both mean and extreme precipitation. ''Mean frequency'' was defined as the number of wet days (precipitation ≥ 1 mm), ''mean intensity'' was defined as the ratio of annual totals to the number of wet days, and ''mean totals'' were defined as annual total or annual mean precipitation. Similarly, ''extreme frequency'' was defined as number of days with precipitation above an absolute threshold (such as 20 mm in the case of the R20mm ETCCDI index), ''extreme intensity'' was defined as annual maximum daily precipitation or annual maximum consecutive 5-day precipitation, and ''extreme totals'' were defined as the annual total precipitation amount from days above an absolute threshold. Note that the ETCCDI indices R95p and R99p are representative of extreme totals since according to ETCCDI the thresholds are calculated based on a climatology (typically 1961–90), meaning the thresholds do not vary on an annual basis. Many remaining parts of the globe have been subject to only isolated studies, usually based on results of regional workshops where invited local participants brought raw station data that were subject to quality control and used to calculate the standard set of ETCCDI indices (e.g., Aguilar et al. 2005, 2009; New et al. 2006; Stephenson et al. 2014; Zhang et al. 2005; Caesar et al. 2011; Vincent et al. 2011; Haylock et al. 2006; Donat et al. 2014). Due to the singular nature of these studies none of the changes demonstrated in them satisfied our definition of ''high confidence.'' Even in cases where multiple studies investigated the same regions there were often conflicting results due to the sparse network of stations used in these studies.

Disentangling the effects of frequency versus intensity changes on global precipitation changes is relevant to discussions on precipitation changes. Trenberth et al. (2003), Trenberth (2011), and Dai et al. (2020) all noted that to fully characterize precipitation changes, frequency, intensity, and duration changes must be examined in addition to changes in accumulated totals. Trenberth et al. (2003) first hypothesized that, in response to warming, the overall precipitation frequency must decrease while the intensity increases at an average rate according to the CC relationship. In particular, the frequency of light to moderate precipitation changes is projected to decrease over most global areas except for the high latitudes (Dai et al. 2018).

In this study we present a comprehensive analysis of changes in the entire distribution of totals and intensity of precipitation, alongside changes in the frequency of precipitation over global land areas. The analysis is based on a new global dataset of gridded ($1° \times 1°$) daily precipitation based on a dense network

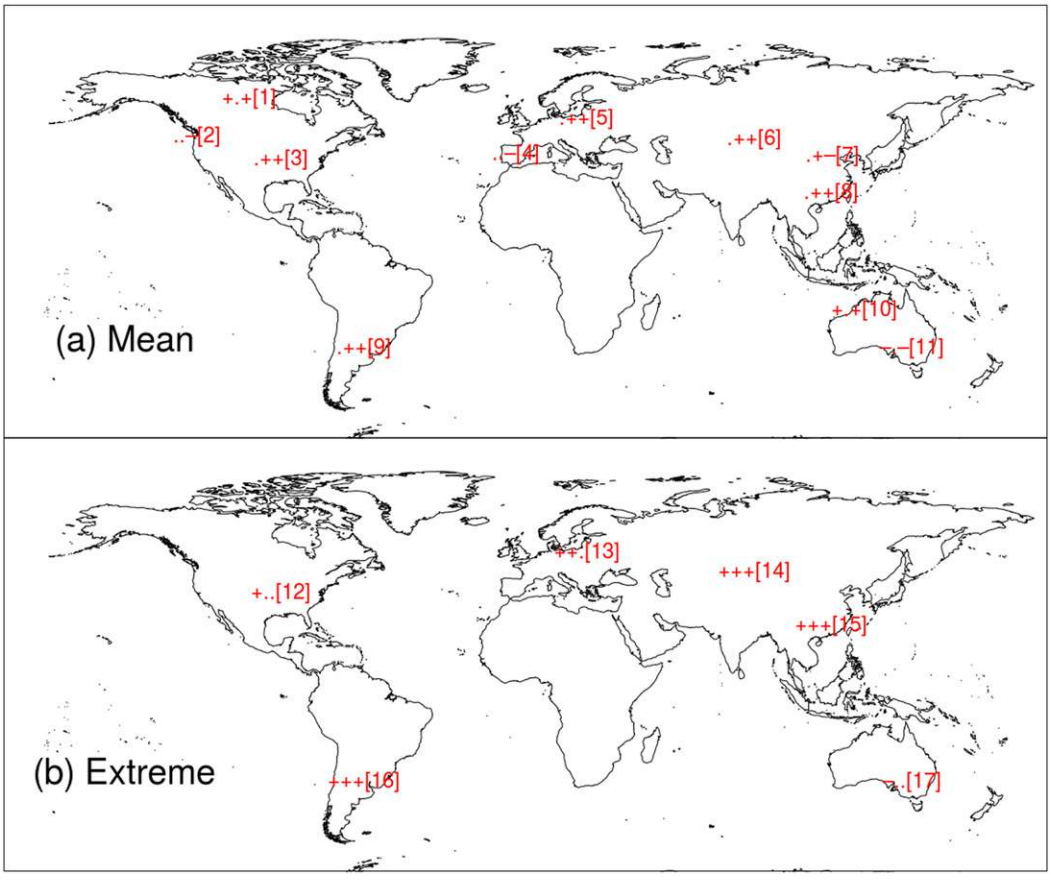

FIG. 1. Summary of regions with high confidence in changes in (a) mean and (b) extreme precipitation frequency, intensity, or totals. The three symbols are related to changes in frequency, intensity, and totals (see text for definitions), respectively, from left to right. The symbols "+", "−", and "." refer to increases, decreases, and unknown (due to a lack of studies, disagreement in literature regarding the direction of change, and/or the changes are not statistically significant) change, respectively. Numbers inside square brackets refer to the references at the end of this caption. High confidence was given to those changes with at least two studies supporting them and no conflicting results between any studies. Regions with unknown changes in all three categories (frequency, intensity, and totals) are not marked. References for numbers are as follows: [1] Vincent and Mekis 2006; Mekis and Vincent 2011; Yagouti et al. 2008; Zhang et al. 2011b; Shephard et al. 2014; [2] Hartmann et al. 2013; Donat et al. 2013b; Kunkel et al. 1999; Groisman et al. 2004; [3] Hartmann et al. 2013; Donat et al. 2013b; Kunkel et al. 1999; Groisman et al. 2004; Higgins and Kousy 2013; Alexander et al. 2006; [4] Hartmann et al. 2013; van den Besselaar et al. 2013; López-Moreno et al. 2010; [5] Hartmann et al. 2013; Klein Tank and Können 2003; Zoline et al. 2009; van den Besselaar et al. 2013; Casanueva et al. 2014; Alexander et al. 2006; Moberg et al. 2006; Donat et al. 2013b; [6] Zhang et al. 2012; Zhai et al. 2005; Ding et al. 2007; Wang et al. 2017; Hu et al. 2017; Wang and Zhou 2005; You et al. 2011; [7] Hartmann et al. 2013; Zhang et al. 2012; Zhai et al. 2005; Ding et al. 2007; [8] Zhai et al. 2005; Ding et al. 2007; You et al. 2011; [9] Haylock et al. 2006; de los Milagros Skansi et al. 2013; Re and Barros 2009; Castañeda and González 2008; Zandonadi et al. 2016; Sarral et al. 2017; [10] Taschetto and England 2009; Shi et al. 2008; Alexander et al. 2006; Hartmann et al. 2013; Contractor et al. 2018; [11] Gallant et al. 2007; Taschetto and England 2009; Groisman et al. 2005; Alexander et al. 2006; Hartmann et al. 2013; Contractor et al. 2018; [12] Donat et al 2013a,b; Kunkel et al. 1999; Groisman et al. 2004; Higgins and Kousky 2013; [13] Klein Tank and Können 2013; Zolina et al. 2009; Alexander et al. 2006; Moberg et al. 2006; Donat et al. 2013a; [14] Zhai et al. 2005; Ding et al. 2007; Wang et al. 2017; Wang and Zhou 2005; You et al. 2011; Yin et al. 2015; [15] Zhai et al. 2005; Ding et al. 2007; Wang and Zhou 2005; Wang and Zhou 2005; [16] Haylock et al. 2006; de los Milagros Skansi et al. 2013; Hartmann et al. 2013; Alexander et al. 2006; [17] Gallant et al. 2007; Groisman et al. 2005; Alexander et al. 2006; Hartmann et al. 2013; Donat et al. 2013a.

of stations from 1950 to 2016, called Rainfall Estimates on a Gridded Network (REGEN) (Contractor et al. 2020). The relatively long temporal record of this dataset allows us to more robustly estimate the climate-scale changes in global observed precipitation, compared to previous studies. The daily temporal resolution preserves the high-frequency extremes and variability while the interpolation removes the bias due to the uneven geographic coverage of stations. Furthermore,

the daily temporal resolution along with a long temporal record of REGEN results in a large sample size of observations, allowing for a robust estimation of the entire distribution of daily precipitation at each grid cell. In addition, REGEN also consists of vital observational uncertainty information, which allows us to identify regions with high-quality observations in this study.

2. Data and methods

a. Gridded daily precipitation data

A newly developed dataset of interpolated daily station precipitation data was used in this study. The dataset is called Rainfall Estimates on a Gridded Network (REGEN) V1–2019 and has global land coverage and covers the period 1950–2016 (Contractor et al. 2020). There are two datasets available under the moniker REGEN. The first interpolates all available daily station data (henceforth REGEN-ALL) while the other interpolates only the stations with 40 complete years of data (henceforth REGEN-40 YR), where a year was considered complete if it contained data for at least 70% of days in each month. This is the same selection criterion as the Global Precipitation Climatology Centre (GPCC) products (Becker et al. 2013). Results in this study are primarily based on REGEN-ALL unless otherwise stated. The main advantage of REGEN is that it is based on a large archive of raw daily station data that allows for a high station density globally extending back to 1950. This archive of raw stations was created by combining the publicly available Global Historical Climatology Network–Daily (GHCN-Daily; Menne et al. 2012) with the equally as large Global Precipitation Climatology Centre archive, which is not publicly shared, along with some smaller archives. An automatic quality control (QC) algorithm developed for GHCN-Daily was applied to the merged data archive to flag potentially low-quality data and subsequently remove flagged data before interpolation [see Durre et al. (2010) for details of the QC algorithm]. We acknowledge that a small percentage of extremes may be falsely flagged and removed in this process.

REGEN has a spatial resolution of $1° \times 1°$ and uses ordinary block kriging interpolation method to generate estimates representative of grid cell average as opposed to point-based estimates. Kriging is a spatial interpolation method that accounts for the spatial autocorrelation structure of precipitation. This method was chosen after a comparison with various popular methods for interpolating precipitation data by Schamm et al. (2014). REGEN also interpolates anomalies (ratios) of daily precipitation to monthly totals that are later converted back to daily totals by multiplying the gridded anomalies with gridded monthly values from GPCC Full Data Monthly V2018 (Ziese et al. 2018). This is known as climatologically aided interpolation (CAI), which 1) reduces the influence of elevation and other covariates (Hofstra et al. 2008), 2) improves the long-term homogeneity since the monthly datasets are based on a more reliable and stable station network, and 3) reduces the effect of individual missing data points compared to gridding absolute values. For more details of the dataset development process and evaluation refer to Contractor et al. (2020). This study utilizes version V1–2019 of the REGEN datasets.

REGEN's station dataset contains the highest number of stations compared to all other existing global daily gauge-based datasets. It was this higher station density that allowed the creation of a gridded dataset with the currently longest temporal record. Currently, no other global gridded daily precipitation datasets exist with a six-decade-long temporal record to enable a robust quasi-global analysis of changes in the entire precipitation distribution. However, temporal inhomogeneities in stations still exist. For example, the majority of stations in India are lost in the early 1970s due to data sharing issues (Contractor et al. 2020). REGEN uses CAI to minimize the effect of temporal inhomogeneities in the station network on the gridded fields. Moreover, Contractor et al. (2020) showed that the temporal average and trends in total annual precipitation and annual maxima compare well between REGEN and a related dataset that utilizes a long-term subset (at least 40 complete years) of stations interpolated by REGEN. REGEN has been evaluated as part of many studies that compare it against various monthly and daily resolution gridded datasets based on rain gauges, satellites, and reanalyses. There were no major artifacts or obvious issues discovered in REGEN by these studies, and REGEN compared very well to existing gauge-based precipitation products over the period of overlap. Please refer to Contractor et al. (2020), Roca et al. (2019), Bador et al. (2020), Alexander et al. (2020), and Hobeichi et al. (2020) for more details.

Besides showing the statistical significance of results for the various calculations, many figures in this study also include a contour enclosing a region where the dataset quality is high. This region was determined based on the three uncertainty estimates included with REGEN: the Yamamoto standard error (Yamamoto 2000), the kriging error, and the number of stations per grid cell. The Yamamoto standard error is indicative of the deviation of the grid cell estimates from the station measurements inside the grid cell, and the kriging error and number of stations inside the grid cell are indicative of the station density inside the grid cell. Although these three dataset uncertainties vary with grid cell and day, a single quality mask was used for the entire dataset based on the temporal average of the three uncertainty estimates. These quality masks are also included with REGEN. For more details on the calculation of the masks, refer to Contractor et al. (2020).

b. Trends in annual and seasonal totals

Trends in annual and seasonal totals of daily precipitation are calculated with a modified Thiel–Sen's slope and the modified Mann–Kendall method is used to test for significance of the trends. ''Modified'' here refers to the modification proposed by Zhang et al. (2000) to account for autocorrelation in the data. Note that this modification was used as a precautionary measure despite not finding any significant temporal autocorrelation at monthly or greater time scales.

The combination of the Thiel–Sen method to estimate slopes and Mann–Kendall test for their significance is advantageous over the most commonly used method for trend

analysis, i.e., least squares regression, as they are nonparametric and as a consequence work with non-Gaussian distributions (such as precipitation). Unlike least squares regression, the Thiel–Sen and Mann–Kendall combination of methods is also compatible with heteroskedastic data. The Theil–Sen method estimates trends by calculating the trends between all pairs of points in the data and then taking the median. As a consequence of its ranking-based methodology, the Thiel–Sen's slope estimate is also insensitive to outliers.

The null hypothesis for the Mann–Kendall test is that there is no monotonic trend while the alternative hypothesis is that there is a monotonic positive or negative trend in the data. The test statistic S computes the sum of the sign change between all pairs of points in the data:

$$S = \sum_{k=1}^{n-1} \sum_{j=k+1}^{n} \text{sign}(X_j - X_k), \tag{1}$$

where

$$\text{sign}(x) = \begin{cases} +1, & \text{for} \quad x > 0 \\ 0, & \text{for} \quad x = 0 \\ -1, & \text{for} \quad x < 0 \end{cases}. \tag{2}$$

The test statistic S is normally distributed under the transformation

$$Z = \begin{cases} \dfrac{S-1}{\sigma}, & \text{for} \quad S > 0 \\ 0, & \text{for} \quad S = 0 \\ \dfrac{S+1}{\sigma}, & \text{for} \quad S < 0 \end{cases} \tag{3}$$

with mean $E[S] = 0$ and variance σ^2 as per Kendall (1975). The null hypothesis is rejected at α% level if the computed Z statistic is outside the $[Z_{-\alpha/2}, Z_{+\alpha/2}]$ interval.

Note that because the Mann–Kendall only tests for a monotonic trend, its results may be sensitive to the period of analysis due to interdecadal variability. However, we include this trend analysis primarily for comparison with previously reported trends in mean precipitation totals in the literature (see Fig. 1a). The main aim of this study is to examine the changes in the frequency and intensity distribution of precipitation. For this we choose to simply calculate a percentage difference in the indices of interest between two long periods, as opposed to calculating trends, which requires satisfying assumptions of linearity of changes.

c. Changes in annual and seasonal frequency

The entire period of data from 1950–2016 was split into two roughly equally long periods (1950–83 and 1984–2016) to test for changes in the number of wet days between the two periods at each grid location. Our aim was to maximize the statistical power of our analysis by choosing the longest possible time periods (thus maximizing the number of observations in each period). The period 1950–2016 was not split exactly equally to avoid unequal number of seasons in each resulting halves. Wet days here are considered as days with at least 1 mm of rainfall since this is the same definition used by ETCCDI (Zhang et al. 2011a). The relative difference in wet day frequency is defined as the difference in the percentage of the number of wet days to the total number of days in each period. For the seasonal calculation, the days considered were restricted to the commonly used definition of seasons: December–February (DJF), March–May (MAM), June–August (JJA), and September–November (SON).

d. Changes in wet-day and all-day distributions

Changes in the wet-day and all-day distributions provide complementary information to understand precipitation changes. As pointed out by Schär et al. (2016), wet-day percentile changes are potentially affected by changes in wet-day frequency, which can complicate their interpretation, while all-day precipitation percentiles are robust to changes in frequency. However, the wet-day quantiles represent the distribution of the daily amount of precipitation conditional on when it rains, and hence are more informative to characterize precipitation intensity changes. Thus, an analysis of changes in frequency (characterized by the number of wet days) alongside changes in the wet-day distribution can help explain the changes in the all-day precipitation distribution. This methodology of characterizing precipitation changes with changes in the entire distribution of wet- and all-day quantiles alongside changes in the number of wet days has been previously used to analyze precipitation changes across Australia (Contractor et al. 2018).

We compared precipitation distributions between 1950–83 and 1984–2016. We chose 300 quantiles, equally spaced between 0 and 1, to represent the wet- and all-day precipitation distributions since the aim was to sample as many parts of the distribution as possible while minimizing the computational resources required and maximizing the statistical power necessary to estimate the highest quantiles. The pth quantile is defined as the value that is expected to exceed a randomly picked sample by a probability p. The last quantile (i.e., 1.0) represents the maximum daily precipitation value in each period (1950–83 and 1984–2016).

The relative change in the pth quantile is given by

$$\Delta q_p = \begin{cases} \dfrac{q_{p_2} - q_{p_1}}{\text{mean}(q_{p_1}, q_{p_2})}, & \text{if} \quad q_{p_1} > 0 \quad \text{and} \quad q_{p_2} > 0 \\ 0, & \text{if} \quad q_{p_1} = q_{p_2} = 0. \end{cases} \tag{4}$$

The second quantile subscript in Eq. (4) refers to the respective periods the quantiles are based on. Note that the statistical power to calculate quantiles reduces substantially in arid regions due to the smaller number of wet days.

e. Changes in the mean daily precipitation intensity

Mean daily precipitation intensity was calculated for each period (1950–83 and 1984–2016) by dividing the total precipitation over the entire time period by the total number of wet days over the entire time period. A relative difference between the two periods was calculated using the following equation at each grid location resulting in a global map of daily precipitation intensity changes (Fig. 7):

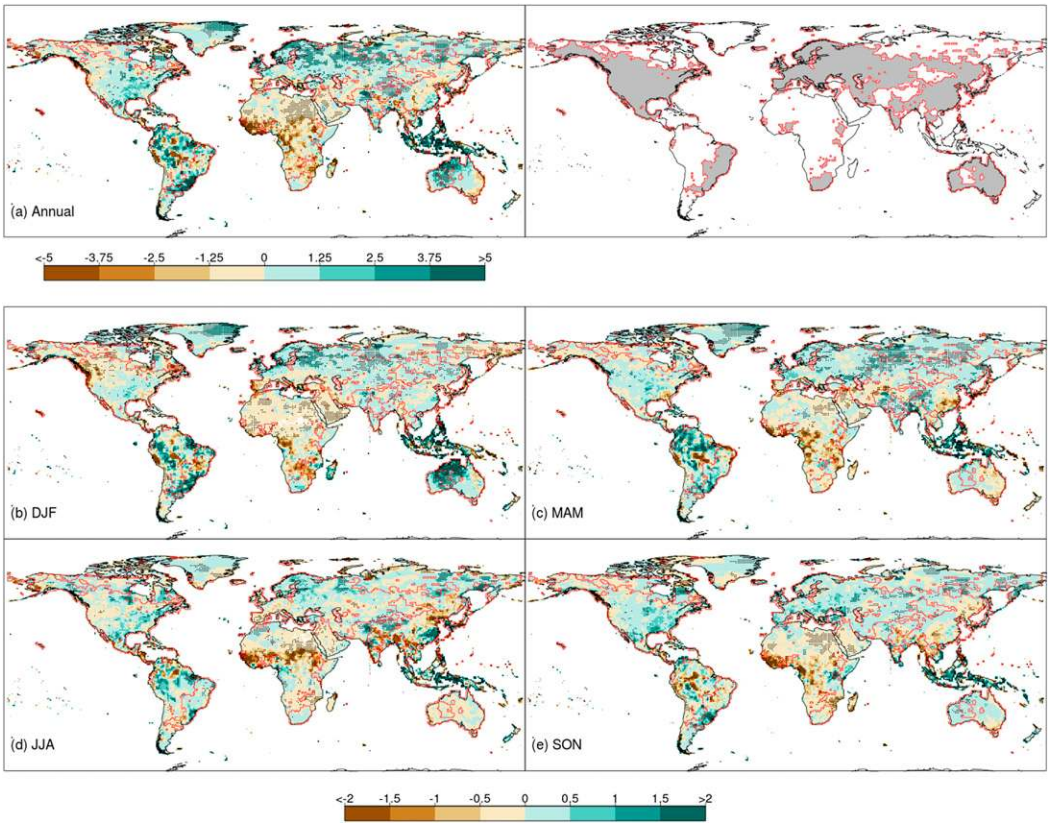

FIG. 2. Trends over 1950–2016 in (a) annual (mm yr^{-1}) and (b)–(e) seasonal (mm $season^{-1}$) totals of daily precipitation data from REGEN-ALL. The stippling indicates significant grids based on modified Mann–Kendall test and the red contours enclose the grids with high-quality observations (see text for details). (top right) Shaded regions identify the data quality mask, and the white (empty) land grids in seasonal changes are due to too few wet days for calculating trends.

$$\Delta I = \begin{cases} \dfrac{I_{p_2} - I_{p_1}}{\text{mean}(I_{p_1}, I_{p_2})}, & \text{if} \quad I_{p_1} > 0 \quad \text{and} \quad I_{p_2} > 0 \\ 0, & \text{if} \quad I_{p_1} = I_{p_1} = 0 \end{cases} . \quad (5)$$

f. Significance testing using bootstrapping

The significance of the changes in frequency, intensity, and quantiles between the two periods was calculated using a bootstrapping technique. A number of daily precipitation records equal to the number of days in each period were sampled from the entire time period (1950–2016) with replacement to create two new resampled time series corresponding to each period (1950–83 and 1984–2016). The resampling was done in two yearly blocks and in the same order for each spatial location to adjust for the spatial and temporal autocorrelation in the data. Subsequently, the relative quantile changes were calculated based on the resampled time periods. This process was repeated 1000 times to create a distribution of relative change in each quantile corresponding to the null hypothesis of no change in the respective quantile. The alternative hypothesis that there has been a significant change in a respective quantile is accepted at a 10% significance level if the true quantile change lies outside the 5th–95th-percentile confidence interval of the resampled distribution. Note that the estimate of sampling uncertainty from bootstrapping includes the sensitivity to our choice of periods.

3. Results

a. Trends in annual and seasonal totals

The most straightforward method of investigating changes in precipitation is to calculate the trends in annual and seasonal totals as shown in Fig. 2. This method was used, for example, by the IPCC AR5 (Hartmann et al. 2013; Alexander et al. 2006). Figure 2 gives a general indication of the changes in precipitation climatology since 1950 at each grid cell, but is not representative of the daily variability, which is averaged out in the annual and seasonal totals. Annually, increases in the total or mean precipitation amounts can be seen in northwest Australia, the eastern United States, Canada, Scandinavia, eastern Europe/western Russia, southeast South America, and northwestern China, similar to the high confidence changes in literature as summarized by Fig. 1. Other areas of increases in Fig. 2a are the northern United Kingdom and parts of Russia, as shown by Casanueva et al. (2014) and Bulygina et al. (2007)

respectively. Again, similar to the high confidence changes in the literature, decreases in the total annual precipitation amounts are seen in southeast Australia and in southern and central-northern China. Other areas of decreases are western and central-western Africa (Hulme et al. 2001; New et al. 2006; Aguilar et al. 2009), Thailand (Limsakul and Singhruck 2016), and northwest and southeast Iran (Rahimzadeh et al. 2009). The decreases in totals in the northwestern United States and eastern Australia are also similar to the high confidence changes in literature shown in Fig. 1; however, the changes in these regions are not statistically significant. Note that there were significant changes in other parts of the globe as well (e.g., northeast Greenland, northern South America, northern Pakistan, and parts of northern Russia); however, these regions were outside the high-quality areas, which reduces our confidence in these changes. These regions may be subject to large observational uncertainties such as differences in interpolation methods, underlying station networks, measurement instruments, spatial resolution (Contractor et al. 2015, 2018; Gervais et al. 2014; Avila et al. 2015; Dunn et al. 2014). For example, all of the regions with significant changes outside high-quality areas have less than one station per grid cell on average over the entire study period. Note that the purpose of Fig. 2 is not to find new areas representing robust trends in annual or seasonal precipitation as it is not possible to do this based on a single dataset. Instead, the comparison between Figs. 1 and 2 serves as a validation that REGEN is capable of reproducing the known precipitation trends in the literature.

Seasonally, the increasing trends in northwestern Australia and eastern Europe occur mainly in DJF (austral summer and boreal winter). The increasing trends in western Russia are present in the boreal spring (MAM) whereas the increases in the eastern United States and Canada are visible all year round but the largest trends are seen in boreal autumn (SON). The decreases in western and central-western Africa are present in all seasons. In the northwest United States/southwest Canada, significant negative trends are observed in DJF whereas significant positive trends are observed in MAM, which seems to indicate a shift in the timing of precipitation from the boreal winter to boreal spring. In China, the increases over the Tibetan Plateau are strongest over boreal spring and summer. The decreases in southern and northeastern China are strongest in boreal summer and autumn while the decreases in southeastern China are strongest in boreal spring. Note, however, that the station distribution is sparse in the western Tibetan Plateau compared to the rest of China (Contractor et al. 2020). Finally, significant negative trends are seen in the Iberian peninsula (Spain, Portugal) in the boreal summer. Although these trends are also present in the annual totals (Fig. 2a), they were not significant. The northward shift of the transition zone in central Europe (the latitude where the sign of trends shifts from positive to negative in the southward direction) from winter to summer (Zolina et al. 2009; van den Besselaar et al. 2013; Terray and Boé 2013) is also evident.

b. *Changes in annual and seasonal frequency of wet days*

To investigate the variability of daily precipitation around the globe, we begin by investigating the changes in the daily frequency of precipitation (Fig. 3). The changes in the frequency of daily precipitation are more spatially coherent compared to annual and seasonal trends. The spatial pattern of changes in annual frequency of wet days (Fig. 3a) reflects the trends in annual totals (Fig. 2a) everywhere except for the northwestern United States, central-western Africa, southeast South America, and parts of the Maritime Continent (i.e., the tropical region between the Pacific and Indian Oceans). Note that among these regions, only the changes in the northwestern United States are based on high-quality observations. Interestingly the daily precipitation frequency has increased throughout the United States. The annual precipitation trends (Fig. 2) across the United States are also positive; however, note that these trends are mostly not statistically significant ($p > 0.05$). U.S.-wide precipitation increases in wet-day frequency have been reported by Karl and Knight (1998) and Wang et al. (2014). Changes in the timing of precipitation in the northwest United States and southwest Canada noted earlier are also apparent here with daily frequency decreasing in boreal winter and increasing in boreal spring. The contrasting changes between eastern and western China (increases in the west and decreases in the east) visible in Fig. 2 are also present in Fig. 3. These changes are visible all year round except in boreal winter (DJF) but are most prominent in boreal spring (MAM). The global mean percentage difference in annual wet days between the two periods is −0.30%. The mean percentage difference over the tropics (high latitudes) is −0.87% (+0.42%).

c. *Changes in wet-day and all-day distributions*

Changes in several quantiles of the all-day precipitation distribution are presented in Fig. 4. The all-day distribution is the distribution of the daily precipitation totals and as a result represents the combined effect of changes in frequency of wet days and intensity of precipitation. Since precipitation distributions are heavily skewed toward the left, the lower amounts represent the most frequent precipitation (with dry days being the most frequent) and the upper extreme amounts represent the least frequent precipitation. In Fig. 4, the value of the change in all grid cells where both quantiles are zero is set to zero [Eq. (4)]. As a result, in parts of Saharan Africa more than 95% of daily values are 0 mm and around 50% of daily values around most global land areas are 0 mm. On the other end of the spectrum, less than 10% of daily precipitation values are 0 mm in northern South America, the Maritime Continent and northern Russia. Note that all three of these regions are outside the high-quality areas.

The spatial pattern of changes until the 8th decile are similar and reflect the spatial pattern of the trends in annual totals (Fig. 2a). Note that the relative changes in the lower quantiles (quantiles less than around 0.6) can be divided into distinct regions of large increases, large decreases, and no changes. The large changes in these lower quantiles may be a result of the small quantile values (close to 0 mm) relative to the changes in these quantile values. In contrast, for quantiles greater than 0.6, regions with smaller increases or decreases (compared to lower quantile changes) are visible. The spatial pattern of changes in the upper extreme tail (quantiles greater than 0.9) are dissimilar to the trends in annual totals, and are hence also

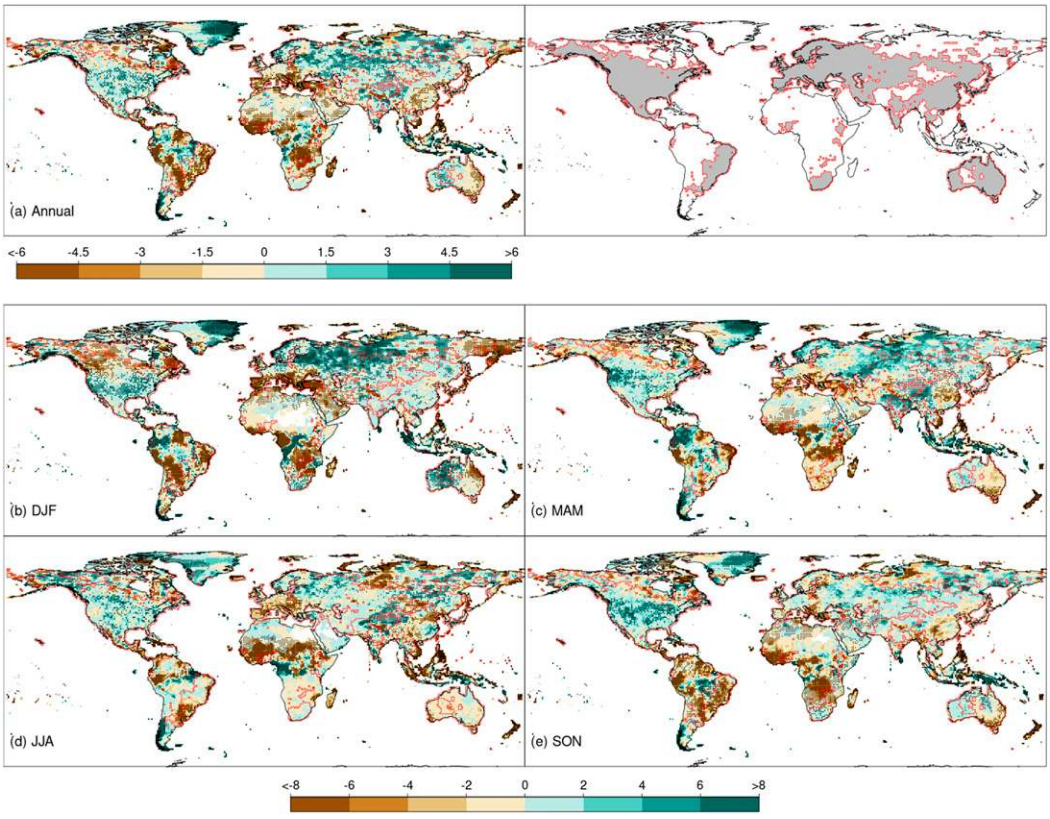

FIG. 3. Difference in (a) annual and (b)–(e) seasonal percentage (%) of wet-day frequency between 1950–83 and 1984–2016 based on REGEN-ALL data. Positive values indicate an increase in wet-day frequency and vice versa. Red contours enclose the grids with high-quality observations (see text for details). The largest positive annual (seasonal) changes are around 27% (30%), and the largest (in absolute magnitude) negative annual (seasonal) changes are around 23% (35%). The white (empty) land grids in seasonal changes in Saharan Africa are due to zero wet days over the entire study period. The stippling indicates grid cells where changes are significant based on the bootstrapping technique described in section 2e.

different from the low to moderate quantiles. For example, compare the changes in the 95th percentile with the seventh decile and Fig. 2a in Spain, the northwestern United States, southeastern Brazil, and southeastern Australia.

A majority of areas show significant increases in the upper extreme quantiles (from around the 90th percentile) than areas that show significant decreases, both inside and outside the high-quality regions (Fig. 6b). Even when averaging the relative all-day quantile changes over land (Fig. 6d) the most extreme quantiles are positive for both all global land areas and for high-quality land areas. Note that most regions with decreases in the upper extreme quantiles are outside the high-quality regions, with the exception of the northwestern United States. This means that the precipitation extremes are increasing in almost all areas where we have high-quality observations around the globe.

To assess the changes in the intensity of precipitation, Fig. 5 shows the changes in the wet-day distribution of precipitation. Note that since the number of wet days vary across grid cells, the same wet-day quantile between grid cells can represent different ''true'' all-day quantiles. The spatial pattern of changes is similar throughout the wet-day distribution (between all panels in Fig. 5). This spatial pattern of changes in the daily wet-day precipitation totals is also very similar to the changes in mean daily precipitation intensity changes (Fig. 7). In general, however, the magnitude of the changes in wet-day quantiles increases from the lower (1st decile) to the upper extreme (99th percentile) quantiles. Throughout the distribution, examples of regions with mainly positive changes are Australia, the Maritime Continent, southeast and northern South America, northern Canada, Scandinavia, and eastern and central Europe. On the other hand, examples of regions with negative changes throughout the distribution are central Africa and northwestern United States. The largest relative changes are found mainly in the middle and equatorial latitudes.

Each panel in Figs. 4 and 5 can be divided into land areas with either positive or negative changes in the respective quantile between the two periods considered. As such Figs. 6a and 6b (top panels) show the difference in the proportion of land showing positive versus negative changes for each quantile. The bottom panels (Figs. 6c,d), instead, show the area-

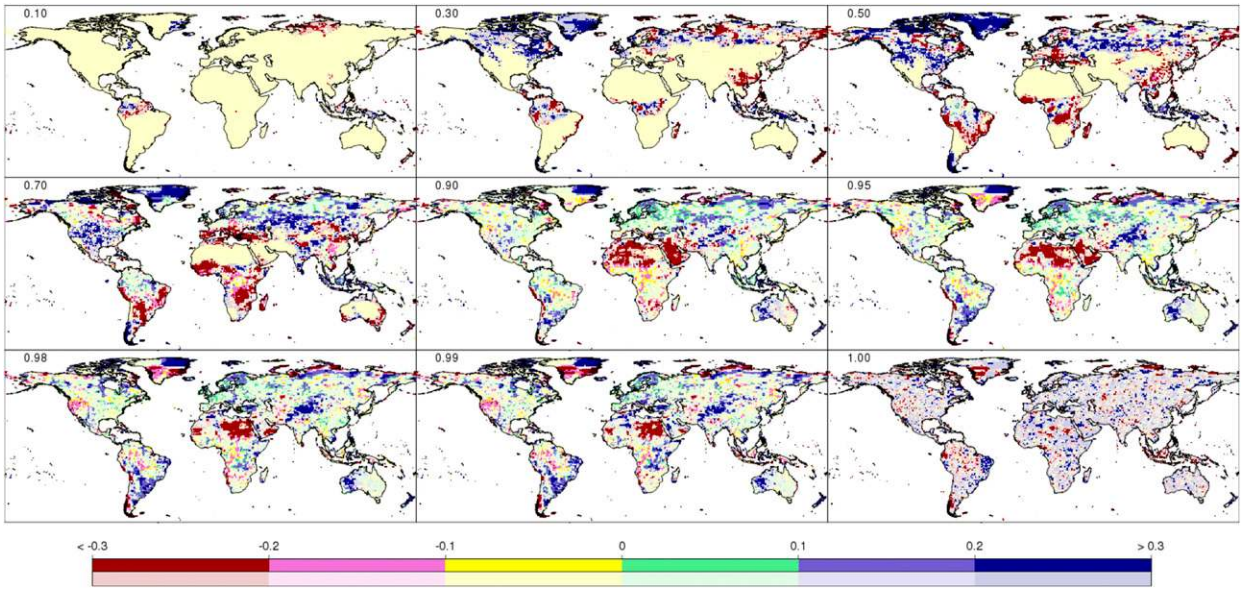

FIG. 4. Changes in quantiles (as indicated by number in the top-left corner of each panel) of all-day precipitation distributions at each grid cell between 1950–83 and 1984–2016, based on REGEN-ALL data. For example, 0.10 indicates the 1st decile and 0.99 indicates the 99th percentile; 1.0 refers to the changes in the maximum daily precipitation value in each period. The faded color scale represents the nonsignificant grid cells and vice versa. Significance testing was done with bootstrapping using a two-tailed test of the null hypothesis of no change at the 10% level (see text for details). The large yellow regions in the former part of the distribution refer to the areas where the quantiles in both periods were zero. Changes are calculated based on Eq. (4) and are hence unitless.

weighted mean of each quantile (i.e., of each panel in Figs. 4 and 5). In general, there are more areas around the globe where intensity of precipitation increases between the two time periods than where it decreases throughout the wet-day distribution (Fig. 6a). This means that whether it is light, moderate, or extreme rainfall, there are more areas around the globe that receive more intense precipitation than areas where it rains less intensely. Figure 6a is based only on grid cells showing significant changes, but even when all land areas (including those without statistically significant changes) are

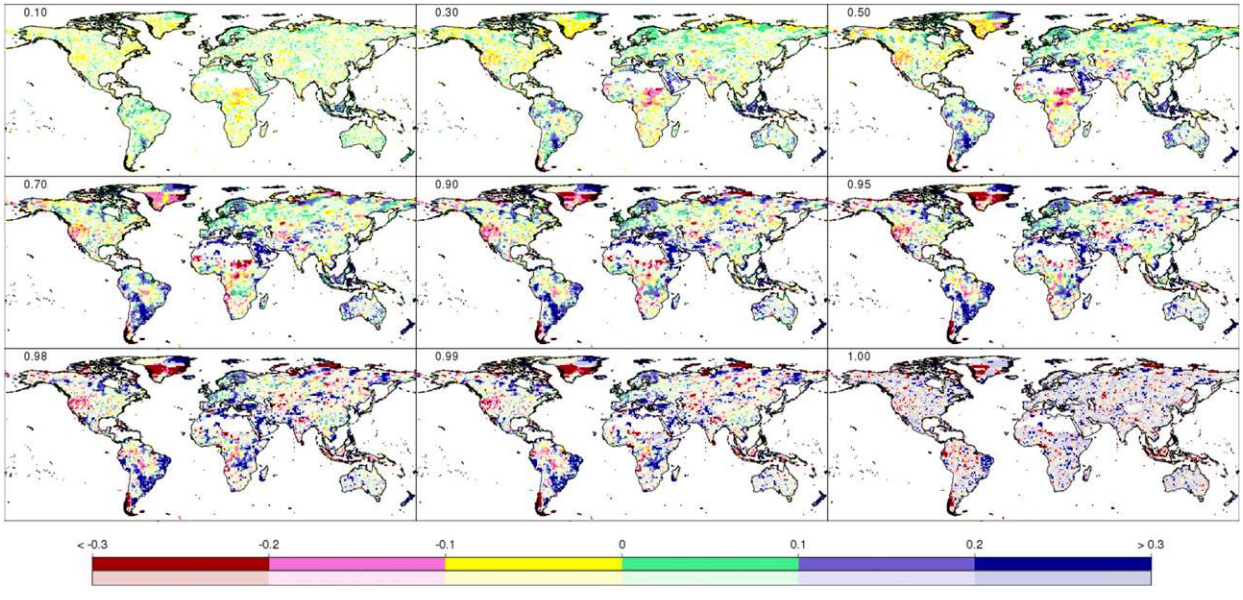

FIG. 5. As in Fig. 4, but for wet-day distributions, that is, changes in quantiles based on time series of wet days (≥1 mm) at each grid cell between 1950–83 and 1984–2016. Faded grids indicate nonsignificant changes. The white (empty) land grid cells had fewer than 300 wet days in each period to allow for robust calculation of 300 quantiles.

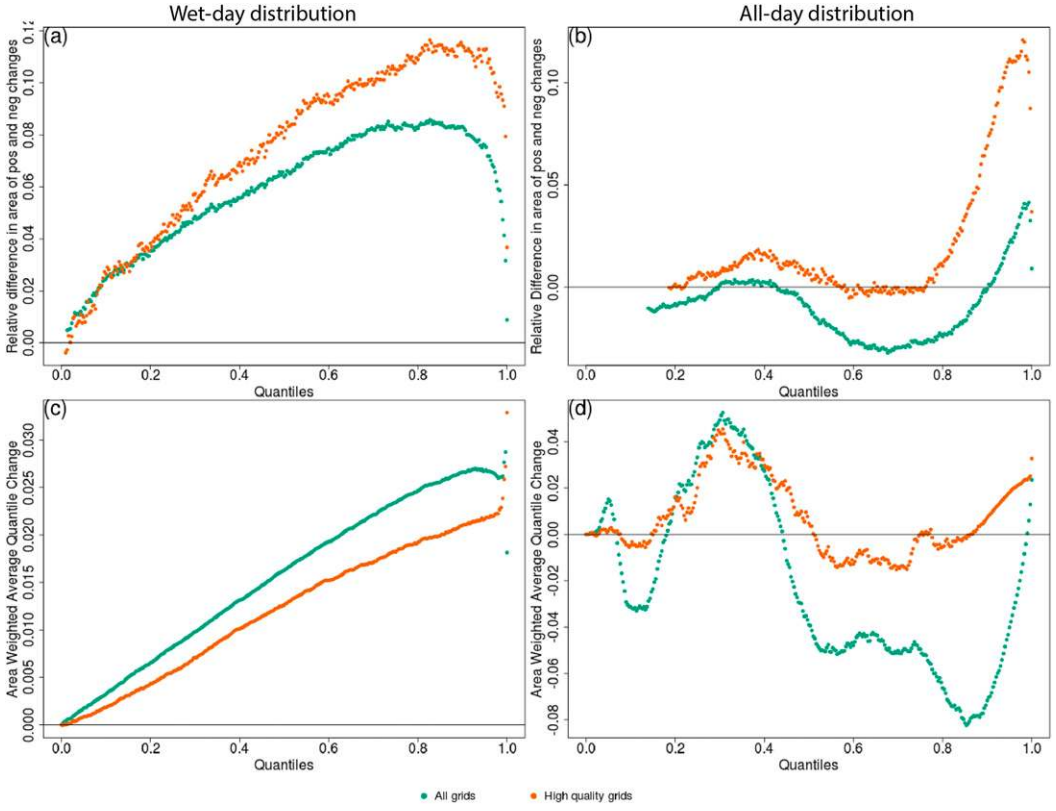

FIG. 6. (top) Difference in the ratios of land areas showing positive and negative changes in quantiles (as seen in Figs. 4 and 5) of (a) the wet-day distribution and (b) the all-day distribution. (bottom) The area-weighted average of the changes in quantiles of (c) the wet-day distribution and (d) the all-day distribution. In all area calculations the grid cells were scaled by a factor of the cosine of the latitude. Colors indicate if the calculations were based on all land-based grid cells or if the calculations were restricted to only those grid cells with high-quality observations according to the data quality mask (see text for details). Only the significant grid cells were used in (a) and (b) while all land grids were used in (c) and (d).

considered, the spatially averaged change in intensity (Fig. 6c) is positive for all quantiles of the wet-day distribution. Since the changes in the uppermost quantiles of the all-day distribution are similar to the changes in the wet-day quantiles, Fig. 6b shows more areas with positive changes in the uppermost extreme quantiles and Fig. 6d shows positive area-weighted average quantile change for the uppermost extreme quantiles. Since there is no spatially widespread increase in intensity evident in the nonextreme all-day quantiles, no meaningful statements can be made based on the low to moderate quantiles in Figs. 6b and 6d.

d. Spatial covariation between frequency and intensity changes in precipitation

Extreme frequency and extreme intensity covary across most land areas (Fig. 8b), whereas no such relationship is evident between mean frequency and mean intensity (Fig. 8a). Areas where extreme frequency and intensity are declining include the Maritime Continent, western Africa, northwestern and southwestern South America, the northwestern United States, large parts of Asia including northern India, the Tibetan Plateau, and northeastern China. Areas where extreme frequency and intensity are increasing include Western Australia, southern and southeastern China, eastern central Africa, northern North America, and eastern South America. The extreme frequency and intensity increase in 44% of global land areas, whereas the extreme frequency and intensity decrease in 33.3% of global land areas. The remaining land areas show mixed increases and decreases in the extreme frequency and intensity.

4. Discussion

Disentangling the combined effect of the frequency and intensity changes on the daily (all-day) precipitation totals can be complex. Based on the comparison of the spatial pattern of changes in the distribution of daily precipitation totals (Fig. 4) with the changes in annual frequency of wet days (Fig. 3a) and the changes in precipitation intensity (the entire distribution of wet days; Fig. 5), we suggest that the changes in the low to moderate quantiles of daily precipitation (until around the 8th decile) reflect the changes in frequency of wet days and the changes in the extreme wet tail (above the 9th decile) reflect

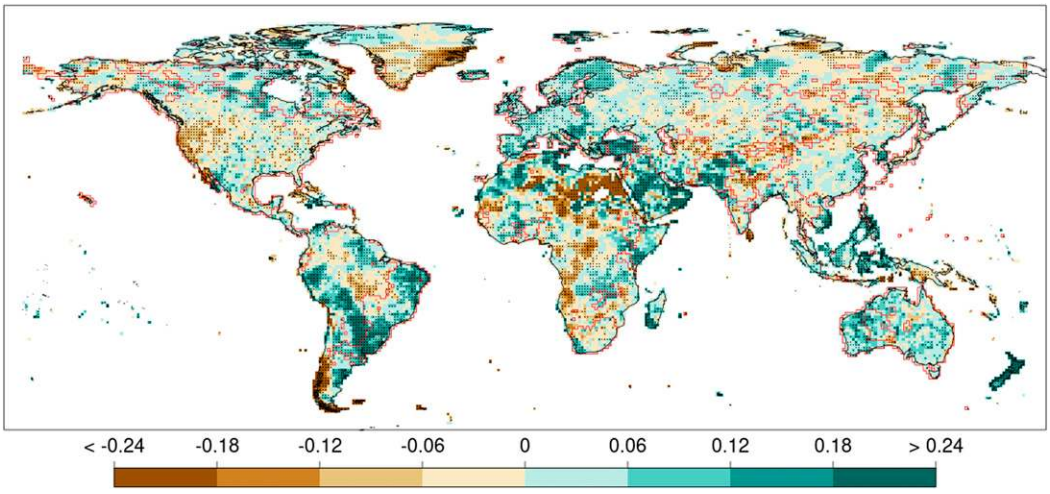

FIG. 7. Relative changes in the mean daily precipitation intensity (ratio of mean annual precipitation intensity in the second period to that in the first). Red contours enclose the grids with high-quality observations. The white (empty) land grid cells had too few wet days in each period for robust calculation of mean intensity changes. The stippling indicates grid cells where changes are significant based on the bootstrapping technique described in section 2e.

the changes in precipitation intensity. Since annual trends in daily precipitation (Fig. 2a) follow changes in the low to moderate all-day quantiles, the spatial pattern of the trends also reflect the changes in frequency of wet days, as noted in section 3b. The only high observational quality regions where trends in annual precipitation totals do not follow the changes in frequency of wet days are the northwestern United States and southeast Brazil. In fact, the annual trends in these regions reflect the changes in precipitation intensity. Furthermore, since the spatial patterns of changes in the entire distribution of precipitation intensity (Fig. 5) are the same, the changes in the average precipitation intensity (Fig. 7) also reflect the changes in the extreme wet tail of the all-day precipitation totals.

When mean frequency or mean intensity changes are viewed in isolation in Fig. 8a, large continental-scale areas can be identified that reflect either coherent increases or decreases in the frequency of wet days or else coherent increases or decreases in average precipitation intensity. For example, the changes in the majority of Asia (including India and China), eastern Europe, and the United States are characterized by increases in frequency of wet days. In contrast, the majority of Europe and Australia are characterized by increases in intensity. Note that Europe and Australia-wide increases are also visible throughout the wet-day precipitation distribution (Fig. 5). Furthermore, since the changes in precipitation intensity reflect the changes in the daily precipitation extremes, a continental-scale increase in daily precipitation extremes is also visible in Europe and Australia (Fig. 4). Although the frequency of wet days and average precipitation intensity have also decreased in many areas around the globe, no large continental-scale regions are apparent where spatially coherent decreases in either the frequency or intensity can be found. The Australia-wide intensification of daily precipitation intensity and daily and subdaily precipitation extremes has been demonstrated by Contractor et al. (2018) and Guerreiro et al. (2018) respectively; however, this study identifies many other regions of continent-wide increases in either frequency of wet days or precipitation intensity (viz., Europe, the United States, and Asia).

Figure 8b shows that the changes (increases or decreases) in the extreme frequency and extreme intensity follow each other. This indicates that there must be a relationship between extreme frequency and extreme intensity, which begs further investigation.

Contractor et al. (2018) also showed, in the context of Australia, that the majority of grid cells showed increases throughout the wet-day distribution from 1958 to 2013, and that the changes in precipitation totals represent the changes in frequency of wet days. In this study, we show that these conclusions also apply across global land areas. Moreover, this study shows that the changes in the daily precipitation extremes in fact represent the changes in precipitation intensity across global land areas. Note that as discussed in section 2d, care must be taken when interpreting changes in wet-day precipitation quantiles as they are affected by changes in frequency.

Modeling studies have shown that total precipitation (A) changes at a rate of $\sim$2% K^{-1}, while precipitation intensity (I) (heavy rainfall rates) follows moisture availability and hence increases at a rate greater or equivalent to the CC rate ($\sim$7% K^{-1}) (Trenberth et al. 2003; Held and Soden 2006; Dai et al. 2020; Pendergrass and Knutti 2018). This means that precipitation frequency (F) must decrease (since $A = F \times I \Rightarrow dA/A = dF/F + dI/I$) (Dai et al. 2020). In particular, modeling studies have shown a decrease in light to moderate precipitation frequency Dai et al. (2018). In agreement with the model-predicted changes in precipitation intensity and mean precipitation frequency, we have shown

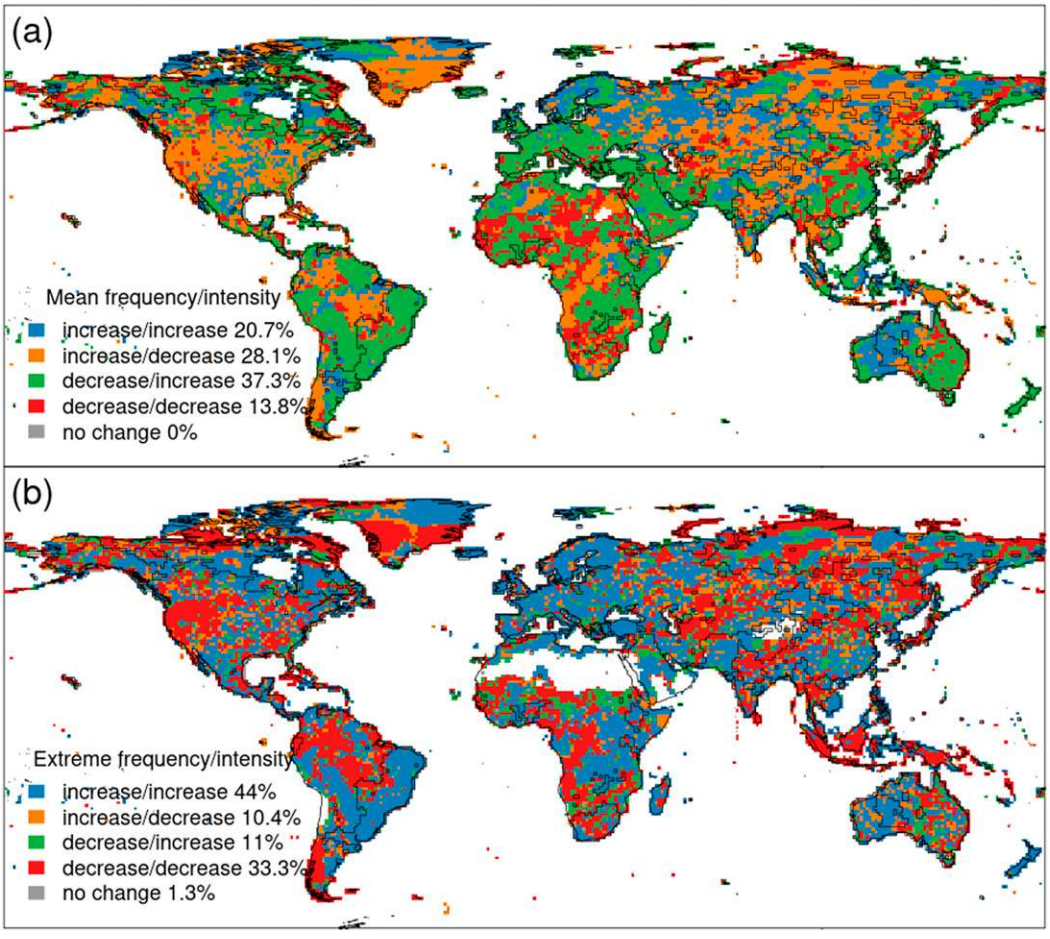

FIG. 8. Concomitant changes in the frequency and intensity of (a) the mean (total) and (b) the extreme precipitation between 1950–83 and 1984–2016. The mean frequency changes were determined by differences in the total number of wet days and the extreme frequency changes were determined by the differences in the number of days with amounts greater than the 99th wet-day percentile in the first period. The mean intensity changes were determined by the differences in the ratios of the total precipitation to the total number of wet days while the extreme intensity changes were determined by the differences in the 99th percentile of the wet-day distribution. The areas enclosed inside black solid contours represent grid cells with high-quality observations (see text for details). The white (empty) land grid cells had too few wet days in each period for robust calculation of mean intensity changes and changes in the 99th wet-day quantile.

based on observational data 1) an increase in the entire distribution of wet-day precipitation intensity (Fig. 5) and 2) a decrease in the number/frequency of wet days (Fig. 3a). Since the extreme tail of the all-day distribution is similar to the wet-day quantiles, this global increase in precipitation intensity is also reflected in the most extreme all-day quantiles. Note, though, that precipitation changes (both extremes and moderate amounts, and precipitation frequency) are not only linked to thermodynamic changes and are likely affected by the interplay of thermodynamic and dynamic drivers (e.g., Pfahl et al. 2017).

The approach of investigating changes in the entire distribution of daily precipitation and intensity, alongside changes in the frequency, can be readily applied to historical and future climate simulations, thus opening new avenues for understanding projected future changes in precipitation. For example, climate models can be used to investigate whether the positive trends in precipitation intensity and precipitation extremes continue into the twenty-first century. Furthermore, historical climate models that are able to simulate the continental-scale increases in frequency of wet days or precipitation intensity (similar to Fig. 8a) can be used to identify the large-scale drivers behind these changes. Changes in these large-scale drivers can then be investigated in climate model simulations over the twenty-first century to determine the effect of a warmer future climate on precipitation in these regions. Similarly the relationships between frequency of wet days and the low to moderate quantiles of the all-day precipitation distribution, the precipitation intensity and the extreme wet tail of the all-day distribution, and extreme frequency and

extreme intensity across global land areas can be investigated in climate model simulations to investigate whether the physical processes behind these relationships change in a warming climate.

This study has been made possible because of spatially consistent analysis using a global dataset of daily precipitation. The identification of similarities in spatial patterns of changes in frequency of wet days and various parts of wet-day and all-day precipitation totals would not have been possible without a sufficiently high-resolution gridded dataset of precipitation such as REGEN. Existing studies based on datasets of indices (Alexander et al. 2006; Donat et al. 2013a,b; Westra et al. 2013) have not allowed for the identification of large regions with consistent changes in precipitation due to their relatively coarse spatial resolution and spatially irregular coverage. More importantly, indices only represent very specific aspects of the precipitation distribution. Availability of daily global gridded data is necessary for such an investigation of changes across the entire distribution of precipitation. Furthermore, it is difficult to confidently assess large-scale changes across land areas using multiple regional studies due to the differences in dataset production and statistical analysis methodologies between them. As a result, regional datasets can also be unsuitable for such an investigation.

Although the station density of REGEN is higher than all existing global gauge-based datasets and datasets of indices, it is still not sufficiently high in many regions such as Africa, South America, Asia, and the Maritime Continent. The 2015 WMO resolution (Alexander 2016) urged countries to exchange daily precipitation records for free for noncommercial research purposes; however, station density remains low in many regions without the ability or a mandate to freely share daily data.

5. Summary and conclusions

Using a newly developed global, land-based dataset of daily precipitation on a $1° \times 1°$ grid from 1950–2016 called REGEN (Contractor et al. 2020), this study demonstrates a comprehensive analysis of changes in the entire distribution of daily precipitation globally. To characterize the changes in the distribution of daily precipitation in terms of frequency and intensity changes, the changes in annual and seasonal frequency of wet days were investigated alongside the changes in the entire distribution of precipitation intensity. Finally, to further understand the spatial variation of mean and extreme precipitation, regional changes were classified based on concomitant changes in the mean/extreme frequency and intensity. Furthermore, we highlight the observational uncertainty of our results by specifying changes for the high observational quality grids in addition to all land grids.

Results from this study show that trends in annual precipitation totals reflect the changes in annual precipitation frequency across all global areas except for the northwestern U.S. and eastern Brazil. More generally, the changes in the low to moderate quantiles (until the 8th decile) of the all-day precipitation distribution reflect changes in frequency of wet days. Continental-scale increases in the frequency of wet days are observed across the majority of Asia, and the United States. Other notable areas showing increases in annual frequency of wet days are the Maritime Continent and western Australia. In contrast, the majority of regions in eastern Australia, southeastern China, southern Europe, Africa, and southeastern South America show decreases in the annual frequency of precipitation.

In comparison, the changes in the precipitation extremes (wet tail of the all-day precipitation distribution) reflect the changes in precipitation intensity. The most notable result of this study is that the majority of land areas show increases throughout the wet-day distribution and the wet tail of the daily precipitation (all-day) distribution. Continental-scale increases in precipitation intensity and extreme precipitation totals are observed across Australia and Europe. The large-scale increases in extreme precipitation and the entire distribution of precipitation intensity (the amount of rainfall when it rains) are consistent with the theoretical expectations for a warming climate based on the Clausius-Clapeyron relationship, although regionally there can be substantial variations in the intensity distribution changes in part related to different changes in dynamical drivers (Pfahl et al. 2017).

Acknowledgments. This study was funded by Australian Research Council (ARC) Grant DP160103439. MGD received funding from ARC Grant DE150100456, and the Spanish Ministry for the Economy, Industry and Competitiveness Grant RYC-2017-22964. LVA was also funded by ARC Grant CE110001028. We are also grateful to the National Centers for Environmental Information (NCEI) and the Global Precipitation Climatology Centre (GPCC) for support during the production of REGEN.

REFERENCES

Adler, R. F., and Coauthors, 2003: The version-2 Global Precipitation Climatology Project (GPCP) monthly precipitation analysis (1979–present). *J. Hydrometeor.*, **4**, 1147–1167, https://doi.org/10.1175/1525-7541(2003)004<1147:TVGPCP>2.0.CO;2.

Aguilar, E., and Coauthors, 2005: Changes in precipitation and temperature extremes in Central America and northern South America, 1961–2003. *J. Geophys. Res.*, **110**, D23107, https://doi.org/10.1029/2005JD006119.

——, and Coauthors, 2009: Changes in temperature and precipitation extremes in western central Africa, Guinea Conakry, and Zimbabwe, 1955–2006. *J. Geophys. Res.*, **114**, D02115, https://doi.org/10.1029/2008JD011010.

Alexander, L. V., 2016: Global observed long-term changes in temperature and precipitation extremes: A review of progress and limitations in IPCC assessments and beyond. *Wea. Climate Extremes*, **11**, 4–16, https://doi.org/10.1016/j.wace.2015.10.007.

——, and Coauthors, 2006: Global observed changes in daily climate extremes of temperature and precipitation. *J. Geophys. Res.*, **111**, D05109, https://doi.org/10.1029/2005JD006290.

——, P. Hope, D. Collins, B. Trewin, A. Lynch, and N. Nicholls, 2007: Trends in Australia's climate means and extremes: A global context. *Aust. Meteor. Mag.*, **56**, 1–18.

——, M. Bador, R. Roca, S. Contractor, M. Donat, and P. L. Nguyen, 2020: Intercomparison of annual precipitation indices and extremes over global land areas from in situ, space-based

and reanalysis products. *Environ. Res. Lett.*, **15**, 055002, https://doi.org/10.1088/1748-9326/ab79e2.

Allen, M. R., and W. J. Ingram, 2002: Constraints on future changes in climate and the hydrologic cycle. *Nature*, **419**, 228–232, https://doi.org/10.1038/nature01092.

Avila, F. B., S. Dong, K. P. Menang, J. Rajczak, M. Renom, M. G. Donat, and L. V. Alexander, 2015: Systematic investigation of gridding-related scaling effects on annual statistics of daily temperature and precipitation maxima: A case study for south-east Australia. *Wea. Climate Extremes*, **9**, 6–16, https://doi.org/10.1016/j.wace.2015.06.003.

Bador, M., L. V. Alexander, S. Contractor, and R. Roca, 2020: Diverse estimates of annual maxima daily precipitation in 22 state-of-the-art quasi-global land observation datasets. *Environ. Res. Lett.*, **15**, 035005, https://doi.org/10.1088/1748-9326/ab6a22.

Becker, A., P. Finger, A. Meyer-Christoffer, B. Rudolf, K. Schamm, U. Schneider, and M. Ziese, 2013: A description of the global land-surface precipitation data products of the Global Precipitation Climatology Centre with sample applications including centennial (trend) analysis from 1901–present. *Earth Syst. Sci. Data*, **5**, 71–99, https://doi.org/10.5194/essd-5-71-2013.

Bhutiyani, M. R., V. S. Kale, and N. J. Pawar, 2010: Climate change and the precipitation variations in the northwestern Himalaya: 1866–2006. *Int. J. Climatol.*, **30**, 535–548, https://doi.org/10.1002/joc.1920.

Bulygina, O. N., V. N. Razuvaev, N. N. Korshunova, and P. Ya. Groisman, 2007: Climate variations and changes in extreme climate events in Russia. *Environ. Res. Lett.*, **2**, 045020, https://doi.org/10.1088/1748-9326/2/4/045020.

Caesar, J., and Coauthors, 2011: Changes in temperature and precipitation extremes over the Indo-Pacific region from 1971 to 2005. *Int. J. Climatol.*, **31**, 791–801, https://doi.org/10.1002/joc.2118.

Casanueva, A., C. Rodríguez-Puebla, M. D. Frías, and N. González-Reviriego, 2014: Variability of extreme precipitation over Europe and its relationships with teleconnection patterns. *Hydrol. Earth Syst. Sci.*, **18**, 709–725, https://doi.org/10.5194/hess-18-709-2014.

Castañeda, M., and M. González, 2008: Statistical analysis of the precipitation trends in the Patagonia region in southern South America. *Atmósfera*, **21**, 303–317.

Chaney, N. W., J. Sheffield, G. Villarini, and E. F. Wood, 2014: Development of a high-resolution gridded daily meteorological dataset over sub-Saharan Africa: Spatial analysis of trends in climate extremes. *J. Climate*, **27**, 5815–5835, https://doi.org/10.1175/JCLI-D-13-00423.1.

Contractor, S., L. V. Alexander, M. G. Donat, and N. Herold, 2015: How well do gridded datasets of observed daily precipitation compare over Australia? *Adv. Meteor.*, **2015**, 1–15, https://doi.org/10.1155/2015/325718.

——, M. G. Donat, and L. V. Alexander, 2018: Intensification of the daily wet day rainfall distribution across Australia. *Geophys. Res. Lett.*, **45**, 8568–8576, https://doi.org/10.1029/2018GL078875.

——, and Coauthors, 2020: Rainfall Estimates on a Gridded Network (REGEN)—A global land-based gridded dataset of daily precipitation from 1950 to 2016. *Hydrol. Earth Syst. Sci.*, **24**, 919–943, https://doi.org/10.5194/hess-24-919-2020.

Dai, A., T. Zhao, and J. Chen, 2018: Climate change and drought: A precipitation and evaporation perspective. *Curr. Climate Change Rep.*, **4**, 301–312, https://doi.org/10.1007/s40641-018-0101-6.

——, R. M. Rasmussen, C. Liu, K. Ikeda, and A. F. Prein, 2020: A new mechanism for warm-season precipitation response to global warming based on convection-permitting simulations. *Climate Dyn.*, **55**, 343–368, https://doi.org/10.1007/s00382-017-3787-6.

de los Milagros Skansi, M., and Coauthors, 2013: Warming and wetting signals emerging from analysis of changes in climate extreme indices over South America. *Global Planet. Change*, **100**, 295–307, https://doi.org/10.1016/j.gloplacha.2012.11.004.

Ding, Y., G. Ren, Z. Zhao, Y. Xu, Y. Luo, Q. Li, and J. Zhang, 2007: Detection, causes and projection of climate change over China: An overview of recent progress. *Adv. Atmos. Sci.*, **24**, 954–971, https://doi.org/10.1007/s00376-007-0954-4.

Donat, M. G., L. V. Alexander, H. Yang, I. Durre, R. Vose, and J. Caesar, 2013a: Global land-based datasets for monitoring climatic extremes. *Bull. Amer. Meteor. Soc.*, **94**, 997–1006, https://doi.org/10.1175/BAMS-D-12-00109.1.

——, and Coauthors, 2013b: Updated analyses of temperature and precipitation extreme indices since the beginning of the twentieth century: The HadEX2 dataset. *J. Geophys. Res. Atmos.*, **118**, 2098–2118, https://doi.org/10.1002/jgrd.50150.

——, and Coauthors, 2014: Changes in extreme temperature and precipitation in the Arab region: Long-term trends and variability related to ENSO and NAO. *Int. J. Climatol.*, **34**, 581–592, https://doi.org/10.1002/joc.3707.

——, A. L. Lowry, L. V. Alexander, P. A. O'Gorman, and N. Maher, 2016: More extreme precipitation in the world's dry and wet regions. *Nat. Climate Change*, **6**, 508–513, https://doi.org/10.1038/nclimate2941.

Dunn, R. J. H., M. G. Donat, and L. V. Alexander, 2014: Investigating uncertainties in global gridded datasets of climate extremes. *Climate Past*, **10**, 2171–2199, https://doi.org/10.5194/cp-10-2171-2014.

Durre, I., M. J. Menne, B. E. Gleason, T. G. Houston, and R. S. Vose, 2010: Comprehensive automated quality assurance of daily surface observations. *J. Appl. Meteor. Climatol.*, **49**, 1615–1633, https://doi.org/10.1175/2010JAMC2375.1.

Gallant, A. J. E., K. J. Hennessy, and J. Risbey, 2007: Trends in rainfall indices for six Australian regions: 1910–2005. *Aust. Meteor. Mag.*, **56**, 223–239.

Gervais, M., L. B. Tremblay, J. R. Gyakum, and E. Atallah, 2014: Representing extremes in a daily gridded precipitation analysis over the United States: Impacts of station density, resolution, and gridding methods. *J. Climate*, **27**, 5201–5218, https://doi.org/10.1175/JCLI-D-13-00319.1.

Groisman, P. Ya., R. W. Knight, T. R. Karl, D. R. Easterling, B. Sun, and J. H. Lawrimore, 2004: Contemporary changes of the hydrological cycle over the contiguous United States: Trends derived from in situ observations. *J. Hydrometeor.*, **5**, 64–85, https://doi.org/10.1175/1525-7541(2004)005<0064:CCOTHC>2.0.CO;2.

——, ——, D. R. Easterling, T. R. Karl, G. C. Hegerl, and V. N. Razuvaev, 2005: Trends in intense precipitation in the climate record. *J. Climate*, **18**, 1326–1350, https://doi.org/10.1175/JCLI3339.1.

Guerreiro, S. B., H. J. Fowler, R. Barbero, S. Westra, G. Lenderink, S. Blenkinsop, E. Lewis, and X.-F. Li, 2018: Detection of continental-scale intensification of hourly rainfall extremes. *Nat. Climate Change*, **8**, 803–807, https://doi.org/10.1038/s41558-018-0245-3.

Guhathakurta, P., and M. Rajeevan, 2008: Trends in the rainfall pattern over India. *Int. J. Climatol.*, **28**, 1453–1469, https://doi.org/10.1002/joc.1640.

Hartmann, D. L., and Coauthors, 2013: Observations: Atmosphere and surface. *Climate Change 2013: The Physical Science Basis*, T. F. Stocker et al., Eds., Cambridge University Press, 159–254, https://doi.org/10.1017/CBO9781107415324.008.

Haylock, M. R., and Coauthors, 2006: Trends in total and extreme South American rainfall in 1960–2000 and links with sea surface temperature. *J. Climate*, **19**, 1490–1512, https://doi.org/10.1175/JCLI3695.1.

Held, I. M., and B. J. Soden, 2006: Robust responses of the hydrologic cycle to global warming. *J. Climate*, **19**, 5686–5699, https://doi.org/10.1175/JCLI3990.1.

Higgins, R. W., and V. E. Kousky, 2013: Changes in observed daily precipitation over the United States between 1950–79 and 1980–2009. *J. Hydrometeor.*, **14**, 105–121, https://doi.org/10.1175/JHM-D-12-062.1.

Hobeichi, S., G. Abramowitz, S. Contractor, and J. Evans, 2020: Evaluating precipitation datasets using surface water and energy budget closure. *J. Hydrometeor.*, **21**, 989–1009, https://doi.org/10.1175/JHM-D-19-0255.1.

Hofstra, N., M. Haylock, M. New, P. Jones, and C. Frei, 2008: Comparison of six methods for the interpolation of daily, European climate data. *J. Geophys. Res.*, **113**, D21110, https://doi.org/10.1029/2008JD010100.

Hu, Z., Q. Zhou, X. Chen, C. Qian, S. Wang, and J. Li, 2017: Variations and changes of annual precipitation in Central Asia over the last century. *Int. J. Climatol.*, **37**, 157–170, https://doi.org/10.1002/joc.4988.

Huffman, G. J., R. F. Adler, M. M. Morrissey, D. T. Bolvin, S. Curtis, R. Joyce, B. McGavock, and J. Susskind, 2001: Global precipitation at one-degree daily resolution from multisatellite observations. *J. Hydrometeor.*, **2**, 36–50, https://doi.org/10.1175/1525-7541(2001)002<0036:GPAODD>2.0.CO;2.

Hulme, M., R. Doherty, T. Ngara, M. New, and D. Lister, 2001: African climate change: 1900–2100. *Climate Res.*, **17**, 145–168, https://doi.org/10.3354/cr017145.

Jain, S. K., V. Kumar, and M. Saharia, 2013: Analysis of rainfall and temperature trends in northeast India. *Int. J. Climatol.*, **33**, 968–978, https://doi.org/10.1002/joc.3483.

Karl, T. R., and R. W. Knight, 1998: Secular trends of precipitation amount, frequency, and intensity in the United States. *Bull. Amer. Meteor. Soc.*, **79**, 231–241, https://doi.org/10.1175/1520-0477(1998)079<0231:STOPAF>2.0.CO;2.

Kendall, M. G., 1975: *Rank Correlation Methods*. Griffin, 202 pp.

Kishore, P., S. Jyothi, G. Basha, S. V. Rao, M. Rajeevan, I. Velicogna, and T. C. Sutterley, 2016: Precipitation climatology over India: Validation with observations and reanalysis datasets and spatial trends. *Climate Dyn.*, **46**, 541–556, https://doi.org/10.1007/s00382-015-2597-y.

Klein Tank, A. M. G., and G. P. Können, 2003: Trends in indices of daily temperature and precipitation extremes in Europe, 1946–99. *J. Climate*, **16**, 3665–3680, https://doi.org/10.1175/1520-0442(2003)016<3665:TIIODT>2.0.CO;2.

Kruger, A. C., 2006: Observed trends in daily precipitation indices in South Africa: 1910–2004. *Int. J. Climatol.*, **26**, 2275–2285, https://doi.org/10.1002/joc.1368.

——, and M. P. Nxumalo, 2017: Historical rainfall trends in South Africa: 1921–2015. *Water SA*, **43**, 285–297, https://doi.org/10.4314/wsa.v43i2.12.

Kunkel, K. E., K. Andsager, and D. D. R. Easterling, 1999: Long-term trends in extreme precipitation events over the conterminous United States and Canada. *J. Climate*, **12**, 2515–2527, https://doi.org/10.1175/1520-0442(1999)012<2515:LTTIEP>2.0.CO;2.

Liebmann, B., and Coauthors, 2014: Understanding recent eastern Horn of Africa rainfall variability and change. *J. Climate*, **27**, 8630–8645, https://doi.org/10.1175/JCLI-D-13-00714.1.

Limsakul, A., and P. Singhruck, 2016: Long-term trends and variability of total and extreme precipitation in Thailand. *Atmos. Res.*, **169**, 301–317, https://doi.org/10.1016/j.atmosres.2015.10.015.

López-Moreno, J. I., S. M. Vicente-Serrano, M. Angulo-Martínez, S. Beguería, and A. Kenawy, 2010: Trends in daily precipitation on the northeastern Iberian Peninsula, 1955–2006. *Int. J. Climatol.*, **30**, 1026–1041, https://doi.org/10.1002/joc.1945.

MacKellar, N., M. New, and C. Jack, 2014: Observed and modelled trends in rainfall and temperature for South Africa: 1960–2010. *S. Afr. J. Sci.*, **110** (7/8), 1–13, https://doi.org/10.1590/sajs.2014/20130353.

Manton, M. J., and Coauthors, 2001: Trends in extreme daily rainfall and temperature in Southeast Asia and the South Pacific: 1961–1998. *Int. J. Climatol.*, **21**, 269–284, https://doi.org/10.1002/joc.610.

Mayowa, O. O., S. H. Pour, and S. Shahid, M. Mohsenipour, S. B. Harun, A. Heryansyah, and T. Ismail, 2015: Trends in rainfall and rainfall-related extremes in the east coast of peninsular Malaysia. *J. Earth Syst. Sci.*, **124**, 1609–1622, https://doi.org/10.1007/s12040-015-0639-9.

Mekis, E., and L. A. Vincent, 2011: An overview of the second generation adjusted daily precipitation dataset for trend analysis in Canada. *Atmos.–Ocean*, **49**, 163–177, https://doi.org/10.1080/07055900.2011.583910.

Menne, M. J., I. Durre, R. S. Vose, B. E. Gleason, and T. G. Houston, 2012: An overview of the Global Historical Climatology Network–Daily database. *J. Atmos. Oceanic Technol.*, **29**, 897–910, https://doi.org/10.1175/JTECH-D-11-00103.1.

Mitchell, T. D., and P. D. Jones, 2005: An improved method of constructing a database of monthly climate observations and associated high-resolution grids. *Int. J. Climatol.*, **25**, 693–712, https://doi.org/10.1002/joc.1181.

Moberg, A., and Coauthors, 2006: Indices for daily temperature and precipitation extremes in Europe analyzed for the period 1901–2000. *J. Geophys. Res.*, **111**, D22106, https://doi.org/10.1029/2006JD007103.

Mondal, A., D. Khare, and S. Kundu, 2015: Spatial and temporal analysis of rainfall and temperature trend of India. *Theor. Appl. Climatol.*, **122**, 143–158, https://doi.org/10.1007/s00704-014-1283-z.

New, M., and Coauthors, 2006: Evidence of trends in daily climate extremes over southern and west Africa. *J. Geophys. Res.*, **111**, D14102, https://doi.org/10.1029/2005JD006289.

O'Gorman, P. A., 2015: Precipitation extremes under climate change. *Curr. Climate Change Rep.*, **1**, 49–59, https://doi.org/10.1007/s40641-015-0009-3.

Omondi, P. A., and Coauthors, 2014: Changes in temperature and precipitation extremes over the Greater Horn of Africa region from 1961 to 2010. *Int. J. Climatol.*, **34**, 1262–1277, https://doi.org/10.1002/joc.3763.

Pendergrass, A. G., and R. Knutti, 2018: The uneven nature of daily precipitation and its change. *Geophys. Res. Lett.*, **45**, 11 980–11 988, https://doi.org/10.1029/2018GL080298.

Peterson, T. C., and R. S. Vose, 1997: An overview of the Global Historical Climatology Network temperature database. *Bull. Amer. Meteor. Soc.*, **78**, 2837–2850, https://doi.org/10.1175/1520-0477(1997)078<2837:AOOTGH>2.0.CO;2.

——, and M. J. Manton, 2008: Monitoring changes in climate extremes: A tale of international collaboration. *Bull. Amer. Meteor. Soc.*, **89**, 1266–1271, https://doi.org/10.1175/2008BAMS2501.1.

Pfahl, S., P. A. O'Gorman, E. M. Fischer, P. A. O'Gorman, and E. M. Fischer, 2017: Understanding the regional pattern of projected future changes in extreme precipitation. *Nat. Climate Change*, **7**, 423–427, https://doi.org/10.1038/nclimate3287.

Rahimzadeh, F., A. Asgari, and E. Fattahi, 2009: Variability of extreme temperature and precipitation in Iran during recent decades. *Int. J. Climatol.*, **29**, 329–343, https://doi.org/10.1002/joc.1739.

Re, M., and V. R. Barros, 2009: Extreme rainfalls in SE South America. *Climatic Change*, **96**, 119–136, https://doi.org/10.1007/s10584-009-9619-x.

Roca, R., L. V. Alexander, G. Potter, M. Bador, R. Jucá, S. Contractor, M. G. Bosilovich, and S. Cloché, 2019: FROGS: A daily 1° × 1° gridded precipitation database of rain gauge, satellite and reanalysis products. *Earth Syst. Sci. Data*, **11**, 1017–1035, https://doi.org/10.5194/essd-11-1017-2019.

Saurral, R. I., I. A. Camilloni, and V. R. Barros, 2017: Low-frequency variability and trends in centennial precipitation stations in southern South America. *Int. J. Climatol.*, **37**, 1774–1793, https://doi.org/10.1002/joc.4810.

Schamm, K., M. Ziese, A. Becker, P. Finger, A. Meyer-Christoffer, U. Schneider, M. Schröder, and P. Stender, 2014: Global gridded precipitation over land: A description of the new GPCC First Guess Daily product. *Earth Syst. Sci. Data*, **6**, 49–60, https://doi.org/10.5194/essd-6-49-2014.

Schär, C., and Coauthors, 2016: Percentile indices for assessing changes in heavy precipitation events. *Climatic Change*, **137**, 201–216, https://doi.org/10.1007/s10584-016-1669-2.

Shephard, M. W., E. Mekis, R. J. Morris, Y. Feng, X. Zhang, K. Kilcup, and R. Fleetwood, 2014: Trends in Canadian short-duration extreme rainfall: Including an intensity-duration-frequency perspective. *Atmos.–Ocean*, **52**, 398–417, https://doi.org/10.1080/07055900.2014.969677.

Shi, G., W. Cai, T. Cowan, J. Ribbe, L. Rotstayn, and M. Dix, 2008: Variability and trend of North West Australia rainfall: Observations and coupled climate modeling. *J. Climate*, **21**, 2938–2959, https://doi.org/10.1175/2007JCLI1908.1.

Smith, T. M., P. A. Arkin, L. Ren, and S. S. P. Shen, 2012: Improved reconstruction of global precipitation since 1900. *J. Atmos. Oceanic Technol.*, **29**, 1505–1517, https://doi.org/10.1175/JTECH-D-12-00001.1.

Stephenson, T. S., and Coauthors, 2014: Changes in extreme temperature and precipitation in the Caribbean region, 1961–2010. *Int. J. Climatol.*, **34**, 2957–2971, https://doi.org/10.1002/joc.3889.

Taschetto, A. S., and M. H. England, 2009: An analysis of late twentieth century trends in Australian rainfall. *Int. J. Climatol.*, **29**, 791–807, https://doi.org/10.1002/joc.1736.

Taylor, K. E., R. J. Stouffer, and G. A. Meehl, 2012: An overview of CMIP5 and the experiment design. *Bull. Amer. Meteor. Soc.*, **93**, 485–498, https://doi.org/10.1175/BAMS-D-11-00094.1.

Terray, L., and J. Boé, 2013: Quantifying 21st-century France climate change and related uncertainties. *C. R. Geosci.*, **345**, 136–149, https://doi.org/10.1016/j.crte.2013.02.003.

Tierney, J. E., C. C. Ummenhofer, and P. B. DeMenocal, 2015: Past and future rainfall in the Horn of Africa. *Sci. Adv.*, **1**, e1500682, https://doi.org/10.1126/sciadv.1500682.

Trenberth, K. E., 1999: Conceptual framework for changes of extremes of the hydrological cycle with climate change. *Climate Change*, **42**, 327–339, https://doi.org/10.1023/A:1005488920935.

——, 2011: Changes in precipitation with climate change. *Climate Res.*, **47**, 123–138, https://doi.org/10.3354/cr00953.

——, A. Dai, R. M. Rasmussen, and D. B. Parsons, 2003: The changing character of precipitation. *Bull. Amer. Meteor. Soc.*, **84**, 1205–1218, https://doi.org/10.1175/BAMS-84-9-1205.

van den Besselaar, E. J. M., A. M. G. Klein Tank, and T. A. Buishand, 2013: Trends in European precipitation extremes over 1951–2010. *Int. J. Climatol.*, **33**, 2682–2689, https://doi.org/10.1002/joc.3619.

Vincent, L. A., and É. Mekis, 2006: Changes in daily and extreme temperature and precipitation indices for Canada over the twentieth century. *Atmos.–Ocean*, **44**, 177–193, https://doi.org/10.3137/ao.440205.

——, and Coauthors, 2011: Observed trends in indices of daily and extreme temperature and precipitation for the countries of the western Indian Ocean, 1961–2008. *J. Geophys. Res.*, **116**, D10108, https://doi.org/10.1029/2010JD015303.

Wang, F., S. Yang, W. Higgins, Q. Li, and Z. Zuo, 2014: Long-term changes in total and extreme precipitation over China and the United States and their links to oceanic-atmospheric features. *Int. J. Climatol.*, **34**, 286–302, https://doi.org/10.1002/joc.3685.

Wang, Y., and L. Zhou, 2005: Observed trends in extreme precipitation events in China during 1961–2001 and the associated changes in large-scale circulation. *Geophys. Res. Lett.*, **32**, L09707, https://doi.org/10.1029/2005GL022574.

——, B. Zhou, D. Qin, J. Wu, R. Gao, and L. Song, 2017: Changes in mean and extreme temperature and precipitation over the arid region of northwestern China: Observation and projection. *Adv. Atmos. Sci.*, **34**, 289–305, https://doi.org/10.1007/s00376-016-6160-5.

Westra, S., L. V. Alexander, and F. W. Zwiers, 2013: Global increasing trends in annual maximum daily precipitation. *J. Climate*, **26**, 3904–3918, https://doi.org/10.1175/JCLI-D-12-00502.1.

Yagouti, A., G. Boulet, L. Vincent, L. Vescovi, and É. Mekis, 2008: Observed changes in daily temperature and precipitation indices for southern Québec, 1960–2005. *Atmos.–Ocean*, **46**, 243–256, https://doi.org/10.3137/ao.460204.

Yamamoto, J. K., 2000: An alternative measure of the reliability of ordinary kriging estimates. *Math. Geol.*, **32**, 489–509, https://doi.org/10.1023/A:1007577916868.

Yin, H., M. G. Donat, L. V. Alexander, and Y. Sun, 2015: Multi-dataset comparison of gridded observed temperature and precipitation extremes over China. *Int. J. Climatol.*, **35**, 2809–2827, https://doi.org/10.1002/joc.4174.

You, Q., and Coauthors, 2011: Changes in daily climate extremes in China and their connection to the large scale atmospheric circulation during 1961–2003. *Climate Dyn.*, **36**, 2399–2417, https://doi.org/10.1007/s00382-009-0735-0.

Zandonadi, L., F. Acquaotta, S. Fratianni, and J. A. Zavattini, 2016: Changes in precipitation extremes in Brazil (Paraná River basin). *Theor. Appl. Climatol.*, **123**, 741–756, https://doi.org/10.1007/s00704-015-1391-4.

Zhai, P., X. Zhang, H. Wan, and X. Pan, 2005: Trends in total precipitation and frequency of daily precipitation extremes over China. *J. Climate*, **18**, 1096–1108, https://doi.org/10.1175/JCLI-3318.1.

Zhang, Q., P. Sun, V. P. Singh, and X. Chen, 2012: Spatial-temporal precipitation changes (1956–2000) and their implications for agriculture in China. *Global Planet. Change*, **82–83**, 86–95, https://doi.org/10.1016/j.gloplacha.2011.12.001.

Zhang, X., L. A. Vincent, W. D. Hogg, and A. Niitsoo, 2000: Temperature and precipitation trends in Canada during the 20th century. *Atmos.–Ocean*, **38**, 395–429, https://doi.org/10.1080/07055900.2000.9649654.

——, and Coauthors, 2005: Trends in Middle East climate extreme indices from 1950 to 2003. *J. Geophys. Res.*, **110**, D22104, https://doi.org/10.1029/2005JD006181.

——, L. Alexander, G. C. Hegerl, P. Jones, A. K. Tank, T. C. Peterson, B. Trewin, and F. W. Zwiers, 2011a: Indices for monitoring changes in extremes based on daily temperature and precipitation data. *Wiley Interdiscip. Rev.: Climate Change*, **2**, 851–870, https://doi.org/10.1002/WCC.147.

——, R. Brown, L. Vincent, W. Skinner, Y. Feng, and E. Mekis, 2011b: Canadian climate trends, 1950-2007. Canadian Biodiversity: Ecosystem Status and Trends 2010, Tech. Thematic Rep. 5, 27 pp., http://www.biodivcanada.ca/default.asp?lang=Enfn&gn=137E1147-0.

Ziese, M., A. Rauthe-Schöch, A. Becker, P. Finger, A. Meyer-Christoffer, and U. Schneider, 2018: GPCC Full Data Daily Version.2018 at 1.0°: Daily Land-Surface Precipitation from Rain-Gauges built on GTS-based and Historic Data. Global Precipitation Climatology Centre, https://www.dwd.de/EN/ourservices/gpcc/gpcc.html.

Zolina, O., C. Simmer, K. Belyaev, A. Kapala, and S. Gulev, 2009: Improving estimates of heavy and extreme precipitation using daily records from European rain gauges. *J. Hydrometeor.*, **10**, 701–716, https://doi.org/10.1175/2008JHM1055.1.